How to cite: *Angew. Chem. Int. Ed.* **2021**, *60*, 22700–22705
International Edition: doi.org/10.1002/anie.202108378
German Edition: doi.org/10.1002/ange.202108378

Mesoporous Materials

Evaporation-Induced Self-Assembly of Small Peptide-Conjugated Silica Nanoparticles

Cornelia von Baeckmann, Guilherme M. D. M. Rubio, Hanspeter Kählig, Dennis Kurzbach, Michael R. Reithofer, and Freddy Kleitz**

Abstract: *Self-assembly processes guide disordered molecules or particles into long-range organized structures due to specific supramolecular interactions among the building entities. Herein, we report a unique evaporation-induced self-assembly (EISA) strategy for four different silica nanoparticle systems obtained through peptide functionalization of the particle surface. First, covalent peptide-silica coupling was investigated in detail, starting with the grafting of a single amino acid (L-serine) and expanded to specific small peptides (up to four amino acids) and transferred to different particle types (MCM-48-type MSNs, solid nanoparticles, and newly developed virus-like nanoparticles). These materials were investigated regarding their ability to undergo EISA, which was shown to be independent of particle type and amount of peptide anchored to their surface. This EISA-based approach provides new possibilities for the design of future advanced drug delivery systems, engineered hierarchical sorbents, and nanocatalyst assemblies.*

Molecular self-assembly is a process which enables a defined arrangement of molecules based on specific, directional, tunable, and non-covalent interactions. Such interactions are typically either electrostatic forces, hydrogen-bonding, aromatic π–π stacking, or van der Waals interactions.[1] In supramolecular chemistry, self-assembly strategies are powerful tools for creating different molecular topologies at the nanoscale.[2] Similarly, Kotov et al. defined the self-assembly of nanoparticles as a process in which the materials acquire non-random spatial distributions.[3] Accordingly, self-assembly of (porous) inorganic or organic-inorganic hybrid nanoparticles into complex functional nanoscale structures could be of high potential in a wide array of applications, such as (nano)catalysis, separation, sensing, bioengineering, controlled drug delivery, and nanomedicine.[4] Several examples demonstrate the growing interest in this area, including the work of Liu et al.,[5] who studied the self-assembly of silica nanoparticles ($\approx$140 nm in diameter) on films using covalent interactions in which the nanoparticles were attached to a substrate via amide bond formation. Also, the use of DNA for programming the self-assembly of nanoparticles is a long-standing field and was already implemented by Storhoff et al. in 1996[6] to develop new types of biosensors. Furthermore, a breakthrough was achieved when the possibility of self-organization through non-covalent interactions between small peptides was demonstrated, especially with diphenylalanine (H-Phe-Phe-OH).[7] The latter peptide is particularly interesting for the present study, since Phe–Phe is known to readily assemble into nanotubes under aqueous conditions due to non-covalent aromatic and hydrogen-bonding interactions. Other types of Phe–Phe morphologies (e.g., spheres, microrods, plate-like crystals, etc.) can be produced through the use of different media or co-assembly techniques.[7c] Moreover, fluorenylmethoxycarbonyl (Fmoc)-protected Phe–Phe may self-assemble into three-dimensional (3D) macroscopic hydrogel nanofiber networks, or, upon slow acidification, into ultrathin membranes of ribbon-like fibers.[8] Based on these properties, small peptides and Fmoc-protected amino acids offer great opportunities to be used as functional materials for cell therapy, tissue engineering, bio-templating, drug delivery, and catalysis,[9] possibly even more so if these small peptides could be combined with nanoparticles.

Self-assembling peptides are exploited here in combination with an evaporation-induced self-assembly (EISA) process—a rapid synthetic approach, to readily access highly ordered long-range hybrid structures.[10] Following the pioneering preparation of ordered mesoporous silica thin films by EISA combined with surfactant-templating,[11] a wide variety of materials could be obtained using this method, such as organosilica hybrids, polymer-silica nanocomposites, films, and monoliths, as well as arrays of gold/CdTe nanoparticles and transition metal oxide structures.[11–13] However, the

[*] C. von Baeckmann, Prof. Dr. F. Kleitz
Department of Inorganic Chemistry—Functional Materials, Faculty of Chemistry, University of Vienna
Währinger Straße 42, 1090 Vienna (Austria)
E-mail: freddy.kleitz@univie.ac.at
G. M. D. M. Rubio, Prof. Dr. M. R. Reithofer
Department of Inorganic Chemistry, Faculty of Chemistry, University of Vienna
Währinger Straße 42, 1090 Vienna (Austria)
E-mail: michael.reithofer@univie.ac.at
Dr. H. Kählig
Department of Organic Chemistry, Faculty of Chemistry, University of Vienna
Währinger Straße 38, 1090 Vienna (Austria)
Prof. Dr. D. Kurzbach
Department of Biological Chemistry, Faculty of Chemistry, University of Vienna
Wahringer Straße 38, 1090 Vienna (Austria)
Supporting information and the ORCID identification number(s) for the author(s) of this article can be found under: https://doi.org/10.1002/anie.202108378.

controlled formation of macroscopic structures using EISA processes involving silica nanoparticles has not been achieved so far.

To achieve this goal, evaporation induced self-assembly of different silica nanoparticles was realized by conjugating a small peptide (Ac-Phe-Phe-OH, peptide **1**, Scheme 1) to the particle surfaces. First, a general strategy for amino acid grafting was developed using Fmoc-protected L-serine. Then, the strategy was adapted to two small peptides (Ac-Phe-Phe-OH and Ac-Lys(Boc)-Asp(O^{t}Bu)-Asp(O^{t}Bu)-Glu(O^{t}Bu)-OH). Initially, reaction conditions were optimized employing MCM-48-type mesoporous silica nanoparticles (MSNs) due to their unique pore properties, their easily functionalizable surface, and the possibility to perform the grafting on the external particle surface only.[14] To investigate the influence of particle size and type, as well as the location of the peptide, on a potential self-assembly event, the procedure was applied to nonporous silica nanoparticles (sNPs), as-made, as well as calcined MCM-48-type MSNs, and newly developed virus-like silica nanoparticles (vlNPs). The produced materials were analyzed using a variety of methods to assess porosity, grafting efficiency, composition, size, and charge of the nanoparticles.

To start, calcined MCM-48-type MSNs were post-functionalized using 3-(amino-propyl)triethoxysilane (APTS) to enable the coupling with carboxylic acids and the formation of amide bonds. Thermogravimetric (TGA) and N_2 physisorption analyses (MCM-48-type MSNs and MCM-48_APTS; Table S1) were in good agreement with previous results.[15] Different coupling reagents for the conjugation of Fmoc-protected serine to MCM-48_APTS were investigated and optimized in terms of coupling efficiency (see Figure S1). For this activation of the carboxylic acid and subsequent amide coupling, the most suitable reagents were 1-hydroxybenzotriazol (HOBt), benzotriazole tetramethyluronium hexafluorophosphate (HBTU), and diisopropylethylamine (DIPEA). The use of 10 equivalents (compared to 1 equiv. of nitrogen, MCM-48_APTS) of serine was found to be crucial to obtain a 6 wt% serine coupling (mass loss by TGA of the MCM-48_APTS = 13 wt% and MCM-48_APTS-serine = 19 wt%). Physisorption analysis revealed that some pores were still accessible in the particles (see Figure S2).

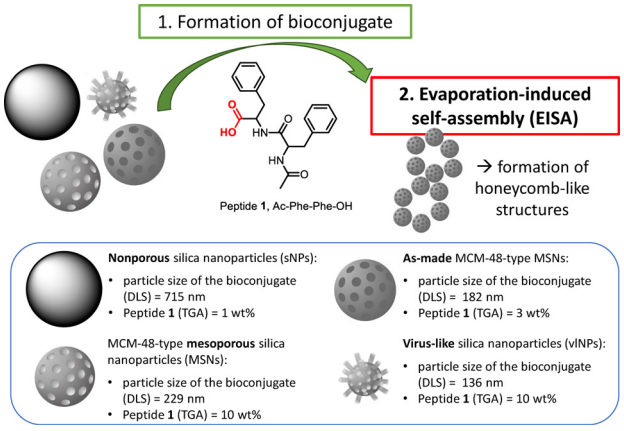

Scheme 1. The EISA process for different types of silica nanoparticles.

Subsequently, peptide **1** (see Scheme 1) was coupled using the same reagents as described above and the successful coupling was confirmed by ^{13}C (CP/MAS) solid-state NMR, TGA, N_2 physisorption analysis (Figure 1), and zeta-potential measurements. Physisorption analysis showed a stepwise decrease in specific surface area, pore volume and pore size with increased functionality, as expected. The zeta-potential decreased from +33 mV for amine-functionalized MSNs to +6 mV after coupling peptide **1** (Figure S3a) due to the introduction of the neutral amide linker. The average hydrodynamic particle diameter increased from 192 ± 6 nm to 223 ± 9 nm due to the presence of the organic species on the external surface (Figure S3b).[15] Furthermore, a stepwise decrease of pore size (19% after APTS functionalization vs. 25% after peptide **1** conjugation), total pore volume (41% vs. 59%) and specific surface area (49% vs. 62%) is clearly visible with increasing degree of functionalization (Figure 1b and Table S1). Using 1 equivalent of peptide **1** resulted in a grafting amount of 10 wt%, while higher peptide quantities resulted in lower efficiency (see Figure 1c). The reason for that is that more solvent was required for the dissolution of the excess peptide, resulting in a more dilute reaction mixture. Detailed results from the physisorption and TGA experiments can be found in the Supporting Information (Table S1). ^{13}C (CP/MAS) ssNMR revealed the dominant peaks resulting from the APTS-functionalized material (9, 22 and 42 ppm; C1, C2 and C3), as well as the existence of the coupled peptide with a broad peak at 172 ppm corresponding to the amide bonds (Figure 1a, C4 and other carbonyls in the peptide). Traces of solvent are observed (three sharp peaks of dimethylformamide (DMF)), which could not be fully

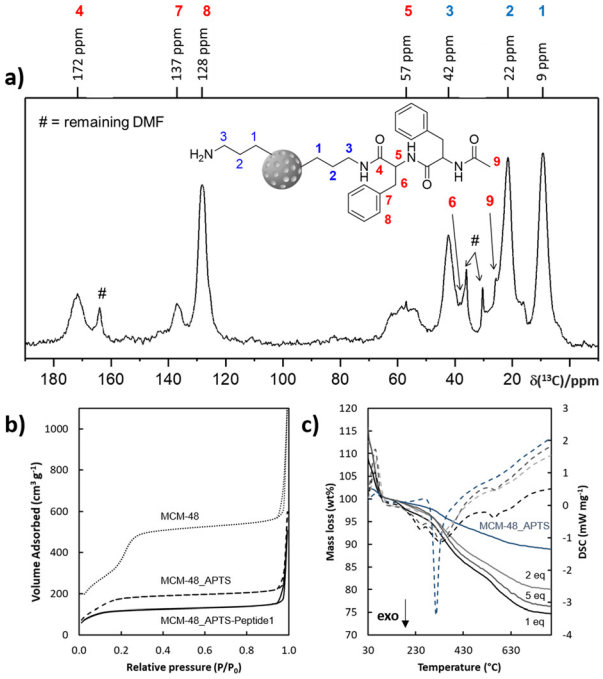

Figure 1. Characterization of the covalently linked peptide **1** onto MCM-48-type MSNs by: a) ^{13}C CP/MAS ssNMR, b) N_2 physisorption measurements (- 196 °C), and c) TGA with different equivalents of peptide **1** used for the coupling.

removed even by extensive washing with dichloromethane (DCM). Furthermore, transmission electron microscopy (TEM) images revealed that the pore structure is preserved throughout the grafting procedure (Figure S4).

Using the optimized conditions (with 1 equiv. of peptide), another larger peptide (Ac-Lys(Boc)-Asp(O^{t}Bu)-Asp-(O^{t}Bu)-Glu(O^{t}Bu)-OH) was coupled to the MSNs to test their feasibility in a generalized conjugation approach. Detailed characterization data can be found in the Supporting Information (Figure S5, S6 and Table S1).

With the optimal conditions in hand, peptide **1** was coupled to 4 different types of particles; MCM-48-type MSNs, as-made-MCM-48, virus-like nanoparticles (vlNPs) and solid nanoparticles (sNPs), as represented in Scheme 1. To obtain a more selective placement of the peptide only on the external surface of MCM-48-type MSNs, as-made materials were used. In this case, the template remains in the pores during the post-grafting of the aminosilane, resulting in MCM-48-type MSNs where the free amine groups are mainly located on the external surface. Consequently, the anchored peptide should also be located mainly on the outer particle surface. According to the physisorption analysis, before and after functionalization with APTS (Figure S7 and Table S2), removal of the template by solvent extraction led to increased specific surface area and pore volume, as well as larger pore size. This increase in porosity corroborates the location of the amine group on the external surface, in addition to reduced pore blocking effects. To verify both the tethering of the amino-silane on the MSNs and the complete removal of the template, ssNMR analysis was carried out (Figure S8). In the ^{13}C (CP/MAS) spectrum, no signals corresponding to the template could be detected. Note that, the material was simply sonicated using an EtOH/HCl mixture directly after the grafting procedure and no complex extraction cycles were needed.[16] The covalent attachment of the silane to the silica network was confirmed by the presence of T-species in the ^{29}Si (CP/MAS) spectrum (Figure S8b). Since the material is treated in EtOH/HCl, ethoxy groups may be present on the surface (when compared to a calcined material), which complicates the exact calculation of added silane based on TGA results. From elemental analysis (EA), the amount of nitrogen was calculated to be 0.84 mmol g^{-1} of silica. After the introduction of the amine groups, the coupling of peptide **1** onto as-made MCM-48-type MSNs was performed as described above and the ^{13}C (CP/MAS) ssNMR was in good agreement with what was observed before (Figure S9).

Virus-like silica nanoparticles were prepared by modifying the synthesis method developed by Zhao et al.[17] All the details concerning the synthetic protocols and the characterization of the particles can be found in the SI (Figures S10-S12 and Tables S3 and S4). In the case of vlNPs-1 especially, small-angle X-ray scattering (SAXS) investigations revealed well-defined oscillations in the scattering pattern representing a very narrow particle size distribution and an average size of 42 nm was calculated (Figure S13). Since the particle size distribution could play a role in the EISA process, the grafting of the peptide was thus performed on vlNPs-1. As before, the particles were functionalized with amine groups (see ^{13}C and ^{29}Si CP/MAS ssNMR spectra in Figure S14), followed by the coupling with peptide **1** (^{13}C CP/MAS spectrum, Figure S15). The amount of APTS was rather low (3 wt% by TGA, Table S5) and ethoxy groups were dominant in the ^{13}C (CP/MAS) ssNMR spectrum indicating incomplete condensation of the silane into the network. The lower amount of APTS was further confirmed by EA (nitrogen 0.38 mmol g^{-1} of silica, Table S7), however it is still found to be sufficient to anchor 10 wt% of peptide **1** (Table S5). As expected, N_2 physisorption analysis of the vlNPs-1 system indicated a decrease in specific surface area with increasing amount of added organic groups (Table S5) while an increase in particle size (from 117 nm to 136 nm for vlNPs-1_APTS-peptide **1**) was observed by dynamic light scattering (DLS). Additionally, as an example of larger particles (580 nm by DLS), solid silica nanoparticles (sNPs) were synthesized using the Stöber method at low temperature.[18] Due to the non-porous character of the particles, the amount of silane anchored was low, and consequently, also the amount of linked peptide **1** (1 wt% by TGA, Table S6). In contrast to the vlNPs-1 (which are considered nonporous as well), the free ethoxy groups after APTS-functionalization were not as dominant in the ^{13}C (CP/MAS) ssNMR spectrum (Figure S16). Since the amount of peptide **1** was low, not all the expected signals could be observed in the ^{13}C (CP/MAS) spectrum (Figure S17), however, the aromatic signals at 128 ppm proved the existence of the peptide on the material.

The self-organization/assembly of these 4 different types of particles was then investigated using scanning electron microscopy (SEM). First, assembly processes in the presence of solvents exhibiting different polarity were examined using sNPs (see Figure S18). Suspensions of sNPs functionalized with peptide **1** were sonicated, followed by deposition on the SEM sample holder. To evaporate the solvent, the sample holder was left in an oven at 100 °C (for the high boiling point solvents) or at room temperature (low boiling point solvents) until complete dryness. No organization could be observed using DCM, tetrahydrofuran (THF), toluene, or ethanol (Figure S18). However, when pentane was used, self-organization and the formation of ring-like structures could be achieved (Figure 2a, right side). Here, it is expected that the intermolecular interactions of the peptide units strongly depend on the type of solvent present, and thus, pentane should not interact/interfere with π–π stacking or hydrogen-bonding processes. In the case of non-functionalized solid silica nanoparticles, simple agglomeration and no assembly could be observed (Figure 2a, left side). Also, the amino-functionalized material was not capable of self-organization (Figure S19).

Interestingly, the same self-assembly behavior was obtained for all the other types of nanoparticles, as can be seen from the SEM images in Figure 2b–d. The obtained architectures appear interconnected, and their structure shows similarities to large honeycombs (Figure 2b). All the materials functionalized with peptide **1** demonstrated EISA into similar honeycomb structures with comparable ring diameters. The average size of the cavities in the honeycomb was calculated using 56 different honeycombs on five SEM images. The resulting mean cavity size was between 4 and 10 μm for all the different particles investigated in this study

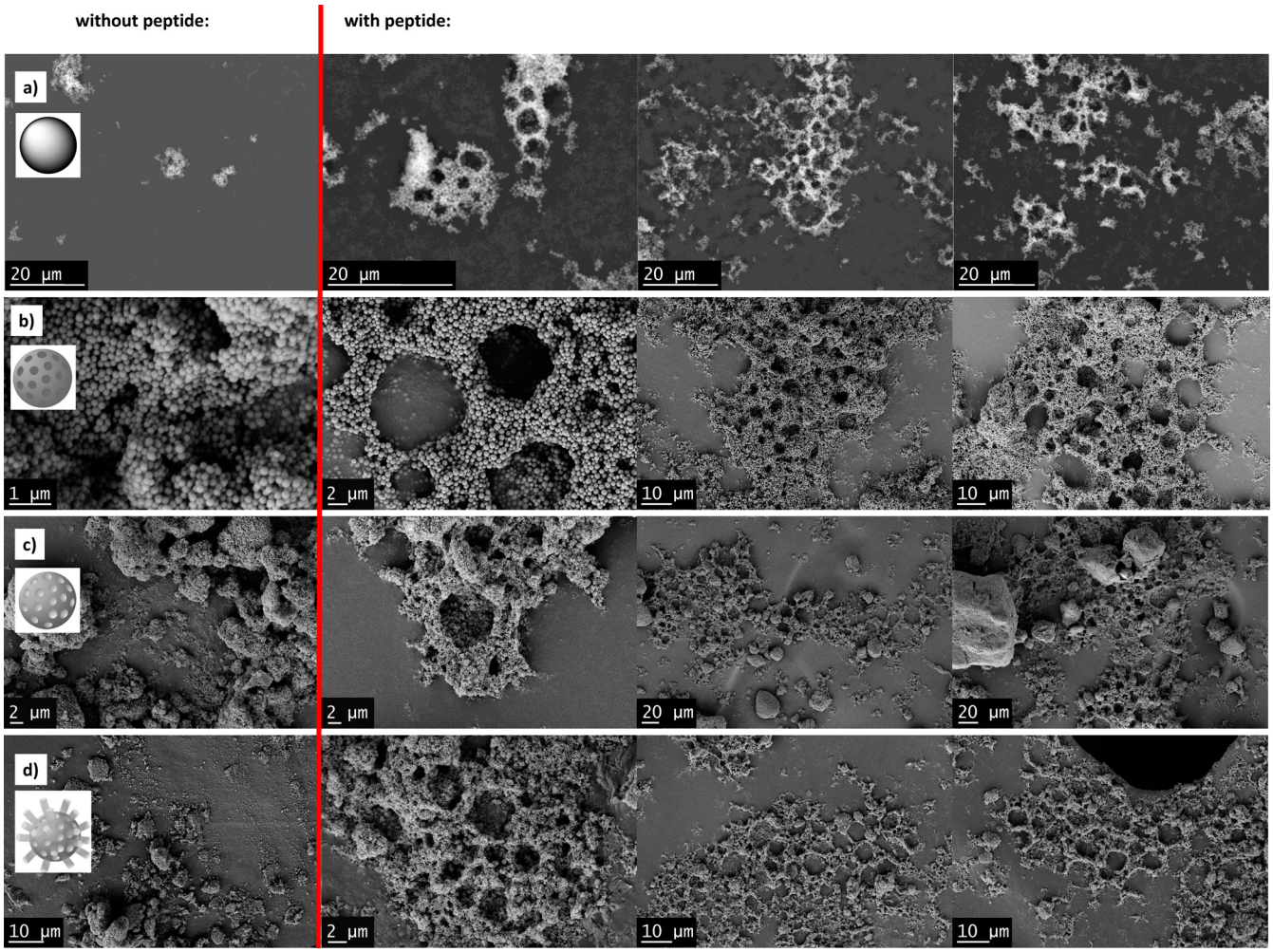

Figure 2. SEM images of the evaporation-induced self-organization of the peptide-silica conjugates using pentane as the solvent: a) sNPs, b) as-made MCM-48-type MSNs, c) MCM-48-type MSNs, and d) vlNPs, conjugated with peptide **1** (on the right), and native material without peptide (on the left).

(4 ± 2 µm for sNPs; 7 ± 4 µm for as-made MCM-48-type MSNs; 6 ± 3 µm for MCM-48-type MSNs; 10 ± 5 µm for vlNPs). From this, one can conclude that the number of particles participating in the formation of a single honeycomb structure is increasing with decreasing particle size. However, the honeycomb structure was sometimes a bit distorted, and the obtained size is an estimation only. Interestingly, honeycomb formation was only observed when pentane was used as solvent, revealing a solvent dependence. Therefore, we could attribute the formation of these micronic cavities to a process similar to breath figure templating,[19] where water-fog microdroplets condense onto a pentane droplet. While pentane has a very low boiling point and high vapor pressure, it evaporates much faster than the water-fog microdroplets condensed onto the pentane surface, resulting in the formation of the observed honeycomb structure. To further assess the packing properties of the particles in these ultrastructures, higher magnification SEM images (Figure S20) and TEM images (Figure S21) were recorded. Both imaging methods confirmed a close-packed structure of the assembly. Interestingly, the microscopy data show some areas of hexagonal close-packing of the particles for vlNPs conjugated with peptide **1**.

A solid-state NMR analysis of peptide **1** grafted onto as-made MCM-48-type MSNs indicated that no major structural adaptions of the dipeptide graft occur due to the self-assembly process (Figure 3a). 2D ^{13}C–^{1}H HetCorr spectra of both the free and assembled forms remained largely unchanged. The only noticeable difference that could be observed was a shoulder appearing up-field (at 119.8 ± 0.4 ppm) to the signals of the aromatic phenylalanine side-chains (bulk at 128.1 ± 0.1 ppm) upon self-assembly (Figure 3b and c). The shoulder could be fitted to a Lorentzian function with a spectral contribution of 6 ± 1% to the overall side-chain signal, indicating that a small fraction (as expected) of the aromatic rings is involved in contact formation between the individual nanoparticles. The strong shift of 9 ppm (bulk vs. shoulder) seems to indicate a significant change in local environment, which might point towards intermolecular π–π interactions and altered ring currents as the underlying force that closely packs the nanoparticles during their aggregation.

In conclusion, EISA of different types of silica nanoparticles into large-scale ring-like structures was accomplished owing to the covalent attachment of a small peptide on the particle surface. The peptide Ac-Phe-Phe-OH was

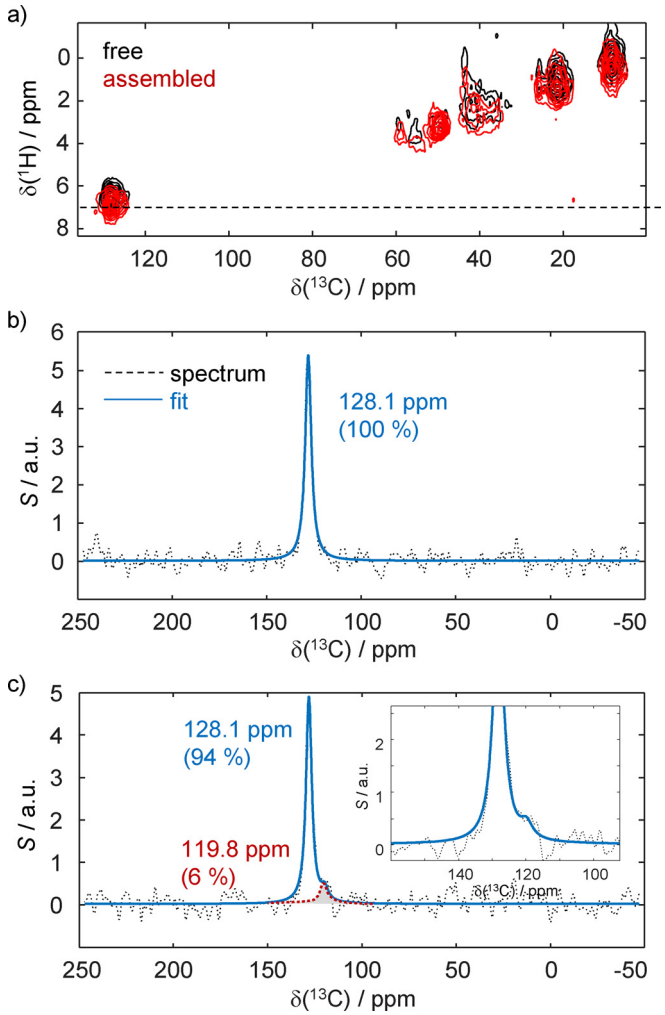

Figure 3. Solid-state NMR analysis of the self-assembly process: a) 2D ^{13}C-^{1}H HetCorr spectra of peptide **1** grafted onto as-made MCM-48-type MSNs in the free (black) and assembled (red) forms. The spectra remain largely unchanged indicating that no major structural adaptions of the dipeptide chains occur as a result of the self-assembly event. b) ^{13}C slice through the 2D spectrum in panel a (indicated by the dashed line) for the free peptide. The spectrum can be fitted to a single Lorentzian (blue line). c) Same as in panel b, but for the self-assembled form. An additional up-field-shifted signal occurs at 119.8 ppm with a 6% spectral contribution.

successfully conjugated on various porous and nonporous nanoparticles. Using suspensions in pentane, the evaporation-induced formation of honeycomb-like structures was achieved with all the tested peptide-conjugated silica particles, demonstrating the general nature of this approach. The self-organization appeared to be independent of the particle size, the particle morphology or the amount of peptide anchored. The bioconjugates described herein, along with their controlled macroscale structuring, provide fundamental insights into assembly processes at different length scales and could pave the way for new concepts that may be useful for the design of smart nanocarriers, stimuli-responsive scaffolds, or bioinspired membranes and nanocatalysts, at the crossroads of material science and biology.

Acknowledgements

The authors acknowledge the funding support of the University of Vienna (Austria). This project was also supported by the Austrian FWF (Stand-alone grant no. P-33338). A project leading to this application (D.K.) received funding from the European Research Council (ERC) under the European Union's Horizon 2020 research and innovation program (grant agreement 801936). The authors thank the NMR center of the Faculty of Chemistry (University of Vienna) for performing liquid NMR experiments, and Mag. Johannes Theiner (University of Vienna) for performing EA.

Conflict of Interest

The authors declare no conflict of interest.

Keywords: conjugation · EISA · peptides · self-organization · silica nanoparticles · solid-state NMR

[1] P. Makam, E. Gazit, *Chem. Soc. Rev.* **2018**, *47*, 3406–3420.
[2] C. J. Brinker, *MRS Bull.* **2004**, *29*, 631–640.
[3] N. A. Kotov, *EPL* **2017**, *119*, 66008.
[4] C. Peng, T. Zeng, Y. Yu, L. Li, R. Wu, *J. Colloid Interface Sci.* **2018**, *531*, 160–167.
[5] Y. An, M. Chen, Q. Xue, W. Liu, *J. Colloid Interface Sci.* **2007**, *311*, 507–513.
[6] a) C. A. Mirkin, R. L. Letsinger, R. C. Mucic, J. J. Storhoff, *Nature* **1996**, *382*, 607–609; b) W. B. Rogers, W. M. Shih, V. N. Manoharan, *Nat. Rev.* **2016**, *1*, 16008.
[7] a) G. Martelli, H. R. Zope, M. B. Capell, A. Kros, *Chem. Commun.* **2013**, *49*, 9932–9934; b) M. Reches, E. Gazit, *Science* **2003**, *300*, 625–627; c) S. Makin, *Nature* **2018**, *559*, S4–S7; d) K. Tao, P. Makam, R. Aizen, E. Gazit, *Science* **2017**, *358*, eaam9756.
[8] H.-G. Braun, A. Z. Cardoso, *Colloids Surf. B* **2012**, *97*, 43–50.
[9] K. Tao, A. Levin, L. Adler-Abramovich, E. Gazit, *Chem. Soc. Rev.* **2016**, *45*, 3935–3953.
[10] H.-P. Cong, S.-H. Yu, *Curr. Opin. Colloid Interface Sci.* **2009**, *14*, 71–80.
[11] a) D. Grosso, F. Cagnol, G. J. de A. A. Soler-Illia, E. L. Crepaldi, H. Amenitsch, A. Brunet-Bruneau, A. Bourgeois, C. Sanchez, *Adv. Funct. Mater.* **2004**, *14*, 309–322; b) T. Fontecave, C. Boissiere, N. Baccile, F. J. Plou, C. Sanchez, *Chem. Mater.* **2013**, *25*, 4671–4678.
[12] a) J. G. Huang, T. Kunitake, S. Onoue, *Chem. Commun.* **2004**, 1008–1009; b) H. Yang, N. Coombs, I. Sokolov, G. A. Ozin, *Nature* **1996**, *381*, 589–592.
[13] a) T. K. Sau, C. J. Murphy, *Langmuir* **2005**, *21*, 2923–2929; b) B. Yuan, L. L. Xing, Y. D. Zhang, Y. Lu, Z. H. Mai, M. Li, *J. Am. Chem. Soc.* **2007**, *129*, 11332–11333; c) Y. Castro, B. Julián-López, C. Boissière, B. Viana, D. Grosso, C. Sanchez, *Microporous Mesoporous Mater.* **2007**, *103*, 273–279; d) T. Brezesinski, B. Smarsly, K.-I. Iimura, D. Grosso, C. Boissière, H. Amenitsch, M. Antonietti, C. Sanchez, *Small* **2005**, *1*, 889–898; e) M. A. Carreon, V. V. Guliants in *Ordered Porous Solids, Vol. 1* (Eds.: V. Valtchev, S. Mintova, M. Tsapatsis), Elsevier Science **2008**, Chapter 16, pp. 413–439.
[14] a) T.-W. Kim, P.-W. Chung, V. S.-Y. Lin, *Chem. Mater.* **2010**, *22*, 5093–5104; b) J. Kecht, A. Schlossbauer, T. Bein, *Chem. Mater.* **2008**, *20*, 7207–7214; c) R. Guillet-Nicolas, A. Popat, J.-L. Bridot, G. Monteith, S. Z. Qiao, F. Kleitz, *Angew. Chem. Int. Ed.* **2013**, *52*, 2318–2322; *Angew. Chem.* **2013**, *125*, 2374–2378;

d) M. Bouchoucha, R. C. -Gaudreault, M.-A. Fortin, F. Kleitz, *Adv. Funct. Mater.* **2014**, *24*, 5911 – 5923.
[15] C. von Baeckmann, R. Guillet-Nicolas, D. Renfer, H. Kählig, F. Kleitz, *ACS Omega* **2018**, *3*, 17496 – 17510.
[16] Y. N. Zhao, S. X. Li, C.-S. Han, *Kor. Chem. Soc.* **2012**, *33*, 3196 – 3202.
[17] W. Wang, P. Wang, X. Tang, A. A. Elzatahry, S. Wang, D. Al-Dahyan, M. Zhao, C. Yao, C.-T. Hung, X. Zhu, T. Zhao, X. Li, F. Zhang, D. Zhao, *ACS Cent. Sci.* **2017**, *3*, 839 – 846.
[18] W. Stöber, A. Funk, E. Bohn, *J. Colloid Interface Sci.* **1968**, *26*, 62 – 69.
[19] a) Y. Sakatani, C. Boissière, D. Grosso, L. Nicole, G. J. A. A. Soler-Illia, C. Sanchez, *Chem. Mater.* **2008**, *20*, 1049 – 1056; b) U. H. F. Bunz, *Adv. Mater.* **2006**, *18*, 973 – 989; c) E. Bormashenko, *Membranes* **2017**, *7*, 45.

Manuscript received: June 23, 2021
Revised manuscript received: August 1, 2021
Version of record online: September 14, 2021

